

A comprehensive study of neutrino spin-flavour conversion in supernovae and the neutrino mass hierarchy

Shin'ichiro Ando[†] and Katsuhiko Sato^{†‡}

[†] Department of Physics, School of Science, The University of Tokyo, 7-3-1 Hongo, Bunkyo-ku, Tokyo 113-0033, Japan

[‡] Research Center for the Early Universe, School of Science, The University of Tokyo, 7-3-1 Hongo, Bunkyo-ku, Tokyo 113-0033, Japan

E-mail: ando@utap.phys.s.u-tokyo.ac.jp

Abstract. Resonant spin-flavour (RSF) conversions of supernova neutrinos, which is induced by the interaction between the nonzero neutrino magnetic moment and supernova magnetic fields, are studied for both normal and inverted mass hierarchy. As the case for the pure matter-induced neutrino oscillation (Mikheyev–Smirnov–Wolfenstein (MSW) effect), we find that the RSF transitions are strongly dependent on the neutrino mass hierarchy as well as the value of θ_{13} . Flavour conversions are solved numerically for various neutrino parameter sets, with presupernova profile calculated by Woosley and Weaver. In particular, it is very interesting that the RSF-induced $\nu_e \rightarrow \bar{\nu}_e$ transition occurs, if the following conditions are all satisfied: the value of $\mu_\nu B$ (μ_ν is the neutrino magnetic moment, and B is the magnetic field strength) is sufficiently strong, the neutrino mass hierarchy is inverted, and the value of θ_{13} is large enough to induce adiabatic MSW resonance. In this case, the strong peak due to original ν_e emitted from neutronization burst would exist in time profile of the neutrino events detected at the Super-Kamiokande detector. If this peak were observed in reality, it would provide fruitful information on the neutrino properties. On the other hand, characters of the neutrino spectra are also different between the neutrino models, but we find that there remains degeneracy among several models. Dependence on presupernova models is also discussed.

PACS numbers: 95.85.Ry, 13.40.Em, 14.60.Pq, 97.60.Bw

1. Introduction

A core-collapse supernova explosion is one of the most spectacular events in astrophysics, and it attracts a great deal of attention from many physicists and astronomers. It also produces a number of neutrinos and 99% of its gravitational binding energy is transformed to neutrinos. Therefore, neutrinos play an essential role in supernovae, and their detection by ground-based large water Čerenkov detectors, such as Super-Kamiokande (SK) and Sudbury Neutrino Observatory (SNO), would provide valuable information on the nature of neutrinos as well as supernova physics. What we can learn from the next galactic supernova has been considered in many articles (for a review, see [1]). For example, we can constrain the properties of neutrino oscillations, such as the mixing angle between the first and third mass eigenstates (θ_{13}), and the mass hierarchy [normal ($m_1 \ll m_3$) or inverted ($m_1 \gg m_3$)] [2, 3].

In addition to the nonzero neutrino masses and mixing angles, the nonzero magnetic moment is another nature of neutrinos beyond the standard model of particle physics. If neutrinos have a nonzero magnetic moment, it leads to precession between left- and right-handed neutrinos in sufficiently strong magnetic fields [4, 5]. In general, nondiagonal elements of the magnetic moment matrix are possible and neutrinos can be changed into different flavours and chiralities [6]. Furthermore, with the additional effect of coherent forward scattering by matter, neutrinos can be resonantly converted into those with different chiralities [7] by a mechanism similar to the well-known Mikheyev–Smirnov–Wolfenstein (MSW) effect [8]. This resonant spin-flavour (RSF) conversion induced by the neutrino magnetic moment in strong magnetic fields was first introduced to solve the solar neutrino problem, and actually gave the best fit solution before the KamLAND result [9]. However, the recent KamLAND experiment [10] has shown that the large mixing angle (LMA) MSW solution is the most favourable one; the RSF mechanism is suppressed at the subdominant level. From the KamLAND negative results for the solar antineutrino search, an upper bound on the neutrino magnetic moment is obtained, $\mu_\nu \lesssim 1 \times 10^{-12} \mu_B$, where μ_B is the Bohr magneton [11]. This upper bound is comparable to the most stringent limit from the stellar cooling argument, $\mu_\nu \lesssim (1-4) \times 10^{-12} \mu_B$ [12].

Although the RSF mechanism does not work at a dominant level in the Sun, it may occur efficiently in a denser environment with stronger magnetic field, which is actually expected in the case of core-collapse supernovae. The RSF conversion mechanism in supernovae has been investigated by many authors [7, 13, 14, 15]. Among them, Ando and Sato [14] have studied the RSF effect using a three-flavour formulation with the latest oscillation parameters, and pointed out that the combination of the MSW and RSF effects makes the crossing scheme very interesting to investigate. Since the RSF conversions are very sensitive to the value of Y_e , which is the electron number fraction per nucleon, they have also investigated the dependence of the RSF effect on presupernova models with solar and zero metallicities [15]. It is concluded that the efficient (either complete or incomplete, depending on presupernova models) RSF conversions occur

when the supernova magnetic field is sufficiently strong, $\mu_\nu B_0 \simeq (10^{-12}\mu_B)(10^{10} \text{ G})$, where B_0 is the strength of the magnetic field at the surface of the iron core.

However, all the past studies of three-flavour RSF effect were based on the assumption that the neutrino mass hierarchy is normal ($m_1 \ll m_3$), although the inverted mass hierarchy ($m_1 \gg m_3$) has not been excluded at all. For the pure MSW effect, it is well-known that the supernova neutrino signal with the case of inverted hierarchy would be very different from that with normal hierarchy [2, 3]. From the analogy of the conversion mechanisms between the MSW and RSF effects, it is easily inferred that the RSF conversions will be also very sensitive to the mass hierarchy. Therefore, in this paper, we study three-flavour RSF conversions with the inverted mass hierarchy using the latest neutrino mixing parameters, and give a comprehensive discussion concerning the dependence on the mass hierarchy. Since the RSF conversions are extremely sensitive to the presupernova models as noted above, we first adopt the model of $15M_\odot$ with solar metallicity by Woosley and Weaver [16] as a reference model; the results with the model by Woosley *et al* [17] with both solar and zero metallicity are addressed later. In particular, we show that the RSF conversion in the case of the inverted hierarchy with the large θ_{13} causes very different neutrino signal from the other models, i.e., the appearance of sharp peak of the neutronization burst in the $\bar{\nu}_e$ time profile. If this case were realized actually, it would be clearly confirmed by not only the neutrino spectrum but also the luminosity curve.

After the completion of our calculation, a paper appeared in which three-flavour RSF effect was studied with both normal and inverted mass hierarchy [18]. The authors studied rather qualitatively, but they did not obtain the result that the neutronization peak in the $\bar{\nu}_e$ signal would be detected, when the efficient RSF conversion takes place in the case of the inverted mass hierarchy and large θ_{13} ; our numerical approach as well as the qualitative discussion clearly indicate that result. Thus, we stress that the point itself is first discovered in the present paper as well as that our study is the first numerical one which comprehensively tackles three-flavour RSF effect with both the normal and inverted mass hierarchy.

This paper is organized as following. In section 2, we give the formulation used in our calculation, which includes all three-flavour neutrinos and antineutrinos. In section 3, models of supernova neutrinos, presupernova structure, and particle properties of the neutrino are illustrated. In section 4, we give qualitative discussions concerning neutrino conversions in supernova matter both for the normal and inverted mass hierarchy, and show results of numerical calculations in section 5. Finally, in section 6, a simple discussion how to obtain information on the neutrino properties from the supernova neutrino signal is presented, and dependence on presupernova models are discussed.

2. Formulation

2.1. Interaction with matter and magnetic fields

The interaction of the magnetic moment of neutrinos and magnetic fields is described by

$$\langle (\nu_i)_R | H_{\text{int}} | (\nu_j)_L \rangle = \mu_{ij} B_{\perp}, \quad (1)$$

where μ_{ij} is the component of the neutrino magnetic moment matrix, B_{\perp} is the magnetic field transverse to the direction of propagation, and $(\nu)_R$ and $(\nu)_L$ are the right- and left-handed neutrinos, respectively. If neutrinos are Dirac particles, right-handed neutrinos and left-handed antineutrinos are undetectable (sterile neutrinos), since they do not interact with matter. On the other hand, if neutrinos are Majorana particles, ν_R are identical to antiparticles of ν_L and interact with matter. In this paper, we assume that neutrinos are Majorana particles. The diagonal magnetic moments are forbidden for Majorana neutrinos, and therefore only conversion between different flavours is possible, e.g., $(\bar{\nu}_e)_R \leftrightarrow (\nu_{\mu,\tau})_L$ or $(\nu_e)_L \leftrightarrow (\bar{\nu}_{\mu,\tau})_R$.

Coherent forward scattering with matter induces an effective potential for neutrinos, which is calculated using weak interaction theory. The effective potential due to scattering with electrons is given by

$$V_{\pm\pm} = \pm\sqrt{2}G_F \left(\pm\frac{1}{2} + 2\sin^2\theta_W \right) n_e, \quad (2)$$

where n_e is the electron number density, G_F is the Fermi coupling constant, and θ_W is the Weinberg angle. The \pm sign in front refers to ν (+) and $\bar{\nu}$ (−) and that in the parentheses to ν_e (+) and $\nu_{\mu,\tau}$ (−). The difference between e and μ, τ neutrinos comes from the existence of charged-current interaction. The subscript $\pm\pm$ of V refers to the first and the second \pm sign. The ordinary MSW effect between ν_e and $\nu_{\mu,\tau}$ is caused by the potential difference $V_e - V_{\mu,\tau} = V_{++} - V_{+-} = \sqrt{2}G_F n_e$, while that between $\bar{\nu}_e$ and $\bar{\nu}_{\mu,\tau}$ by $V_{\bar{e}} - V_{\bar{\mu},\bar{\tau}} = V_{--} - V_{-+} = -\sqrt{2}G_F n_e$. To include the RSF effect, which causes conversion between neutrinos and antineutrinos, we should take into account the neutral-current scattering by nucleons:

$$V = \sqrt{2}G_F \left(\frac{1}{2} - 2\sin^2\theta_W \right) n_p - \sqrt{2}G_F \frac{1}{2} n_n, \quad (3)$$

where n_p, n_n are the proton and neutron number density, respectively. For neutrinos we add $+V$ to the potential and for antineutrinos $-V$. Therefore, the RSF conversion between ν_e and $\bar{\nu}_{\mu,\tau}$, which is important for the case considered in this paper, obeys the potential difference

$$\begin{aligned} \Delta V &\equiv V_e - V_{\bar{\mu},\bar{\tau}} \\ &= (V_{++} + V) - (V_{--} - V) \\ &= -\sqrt{2}G_F \frac{\rho}{m_N} (1 - 2Y_e), \end{aligned} \quad (4)$$

where ρ is the density, m_N is the nucleon mass, and $Y_e = n_e/(n_e + n_n)$ is the number of electrons per baryon. (When we obtained equation (4), we assumed charge neutrality $n_e = n_p$.)

2.2. The simplest case: $\nu_e \leftrightarrow \bar{\nu}'_\tau$ conversion

In this subsection, we give the simplest formulation between ν_e and $\bar{\nu}'_\tau$ with the mass squared difference and mixing angle between the first and third mass eigenstate $\Delta m_{13}^2, \theta_{13}$, and consider the properties of the RSF conversion. Here, $\bar{\nu}'_\tau$ represents mass eigenstate in matter which can be obtained by some linear combination of $\bar{\nu}_\mu$ and $\bar{\nu}_\tau$. Although this treatment is obviously insufficient for a realistic discussion, it is still useful for an intuitive understanding. First, we qualitatively illustrate how the RSF conversions depend on the neutrino mass hierarchy, and then more realistic three-flavour formulation is given in the next subsection. The time evolution of the mixed state of ν_e and $\bar{\nu}'_\tau$ is described by the Schrödinger equation

$$i \frac{d}{dr} \begin{pmatrix} \nu_e \\ \bar{\nu}'_\tau \end{pmatrix} = \begin{pmatrix} 0 & -\mu_{e\tau'} B_\perp \\ -\mu_{e\tau'} B_\perp & \Delta H \end{pmatrix} \begin{pmatrix} \nu_e \\ \bar{\nu}'_\tau \end{pmatrix}, \quad (5)$$

where r is the radius from the center of the star, $\mu_{e\tau'}$ is the transition magnetic moment, and ΔH is defined by

$$\Delta H \equiv \frac{\Delta m_{13}^2}{2E_\nu} \cos 2\theta_{13} - \Delta V. \quad (6)$$

The resonance occurs when $\Delta H = 0$; it does not occur if $\Delta m_{13}^2 > 0$ (normal hierarchy), because $Y_e < 0.5$ (therefore, $\Delta V < 0$) is satisfied in stellar envelope. Instead, the conversion between $\bar{\nu}_e$ and ν_τ is affected by the resonance since the potential difference between them is $V_{\bar{e}} - V_{\mu,\tau} = -\Delta V (> 0)$. On the other hand, in the case of the inverted hierarchy, the RSF conversion takes place between ν_e and $\bar{\nu}'_\tau$, but not between $\bar{\nu}_e$ and ν'_τ . This situation is very similar to the case of pure MSW effect; higher MSW resonance occurs in antineutrino (neutrino) sector if the mass hierarchy is inverted (normal) [2, 3].

When the resonance is adiabatic (or when the density is slowly changing at that point and the magnetic field is strong enough), significant conversion occurs. The adiabaticity of the RSF conversion is given by

$$\gamma_{e\tau'}^{\text{RSF}} = \frac{(2\mu_{e\tau'} B_\perp)^2}{|d\Delta V/dr|} \Big|_{\text{res}}, \quad (7)$$

where the subscript “res” means that the value is evaluated at the resonance point. Therefore, if the magnetic field is sufficiently strong at the resonance point, the $\nu_e \leftrightarrow \bar{\nu}'_\tau$ conversion occurs completely.

2.3. Three-flavour formulation

Here, we present the three-flavour (six-component) formulation of neutrino mixing, on which our discussions depend:

$$i \frac{d}{dr} \begin{pmatrix} \nu \\ \bar{\nu} \end{pmatrix} = \begin{pmatrix} H_0 & B_\perp M \\ -B_\perp M & \bar{H}_0 \end{pmatrix} \begin{pmatrix} \nu \\ \bar{\nu} \end{pmatrix}, \quad (8)$$

where

$$\nu = \begin{pmatrix} \nu_e \\ \nu_\mu \\ \nu_\tau \end{pmatrix}, \quad \bar{\nu} = \begin{pmatrix} \bar{\nu}_e \\ \bar{\nu}_\mu \\ \bar{\nu}_\tau \end{pmatrix}, \quad (9)$$

$$H_0 = \frac{1}{2E_\nu} U \begin{pmatrix} 0 & 0 & 0 \\ 0 & \Delta m_{12}^2 & 0 \\ 0 & 0 & \Delta m_{13}^2 \end{pmatrix} U^\dagger + \begin{pmatrix} V_{++} + V & 0 & 0 \\ 0 & V_{+-} + V & 0 \\ 0 & 0 & V_{+-} + V \end{pmatrix}, \quad (10)$$

$$\bar{H}_0 = \frac{1}{2E_\nu} U \begin{pmatrix} 0 & 0 & 0 \\ 0 & \Delta m_{12}^2 & 0 \\ 0 & 0 & \Delta m_{13}^2 \end{pmatrix} U^\dagger + \begin{pmatrix} V_{-+} - V & 0 & 0 \\ 0 & V_{--} - V & 0 \\ 0 & 0 & V_{--} - V \end{pmatrix}, \quad (11)$$

$$U = \begin{pmatrix} U_{e1} & U_{e2} & U_{e3} \\ U_{\mu 1} & U_{\mu 2} & U_{\mu 3} \\ U_{\tau 1} & U_{\tau 2} & U_{\tau 3} \end{pmatrix} = \begin{pmatrix} c_{12}c_{13} & s_{12}c_{13} & s_{13} \\ -s_{12}c_{23} - c_{12}s_{23}s_{13} & c_{12}c_{23} - s_{12}s_{23}s_{13} & s_{23}c_{13} \\ s_{12}s_{23} - c_{12}c_{23}s_{13} & -c_{12}s_{23} - s_{12}c_{23}s_{13} & c_{23}c_{13} \end{pmatrix}, \quad (12)$$

$$M = \begin{pmatrix} 0 & \mu_{e\mu} & \mu_{e\tau} \\ -\mu_{e\mu} & 0 & \mu_{\mu\tau} \\ -\mu_{e\tau} & -\mu_{\mu\tau} & 0 \end{pmatrix}, \quad (13)$$

and $c_{ij} = \cos \theta_{ij}$, $s_{ij} = \sin \theta_{ij}$. (We assume the CP phase $\delta = 0$ in equation (12) for simplicity.)

The resonant flavour conversion basically occurs when the two diagonal elements in the matrix in equation (8) have the same value. There are four relevant resonance points, but they depend on the neutrino mass hierarchy as discussed in the previous subsection. In the case of the normal mass hierarchy, they are for $\nu_e \leftrightarrow \nu'_\mu$ (MSW-L), $\nu_e \leftrightarrow \nu'_\tau$ (MSW-H), $\bar{\nu}_e \leftrightarrow \nu'_\mu$ (RSF-L), and $\bar{\nu}_e \leftrightarrow \nu'_\tau$ (RSF-H). Here, the quantities such as $\nu'_{\mu,\tau}$ ($\bar{\nu}'_{\mu,\tau}$) represent mass eigenstates in matter which can be obtained by linear combination of ν_μ ($\bar{\nu}_\mu$) and ν_τ ($\bar{\nu}_\tau$). This is because the ν_e ($\bar{\nu}_e$) state coincides with mass eigenstate in matter owing to large matter potential, and the other mass eigenstates are obtained by the rotation of ν_μ ($\bar{\nu}_\mu$) and ν_τ ($\bar{\nu}_\tau$) basis. Suffixes ‘-L’ and ‘-H’ attached to ‘MSW’ and ‘RSF’ indicate whether the density at the resonance points are lower or higher. On the other hand, in the case of the inverted hierarchy, RSF-H occurs for $\nu_e \leftrightarrow \bar{\nu}'_\tau$ as well as MSW-H for $\bar{\nu}_e \leftrightarrow \bar{\nu}'_\tau$, whereas the other two resonances occur for the same conversions. This situation is summarized in table 1.

Table 1. Flavour conversions that are important for each resonance, in both cases of the normal and inverted mass hierarchy.

Resonance	Normal hierarchy	Inverted hierarchy
RSF-H	$\bar{\nu}_e \leftrightarrow \nu'_\tau$	$\nu_e \leftrightarrow \bar{\nu}'_\tau$
RSF-L	$\bar{\nu}_e \leftrightarrow \nu'_\mu$	$\bar{\nu}_e \leftrightarrow \nu'_\mu$
MSW-H	$\nu_e \leftrightarrow \nu'_\tau$	$\bar{\nu}_e \leftrightarrow \bar{\nu}'_\tau$
MSW-L	$\nu_e \leftrightarrow \nu'_\mu$	$\nu_e \leftrightarrow \nu'_\mu$

3. Models

3.1. Original neutrino emission

We adopt, as original neutrino spectrum as well as luminosity curve, the result of numerical simulation by Thompson *et al* [19]; we use the model calculated for the $15M_\odot$ progenitor star. Their calculation has particularly focused on shock breakout and followed the dynamical evolution of the cores through collapse until the first 250 ms after bounce. They have incorporated all the relevant neutrino processes such as neutrino–nucleon scatterings with nucleon recoil as well as nucleon bremsstrahlung; these reactions have recently been recognized to give non-negligible contribution to the spectral formation. In figures 1 and 2, we show the original luminosity curve and number spectrum of neutrinos, respectively. In these figures, ν_x represents non-electron neutrinos and antineutrinos.

Neutrino luminosity curve is quite characteristic among different flavours. In particular, there is a very sharp peak of ν_e called ‘neutronization burst’, whose duration is typically ~ 10 ms and peak luminosity is $\sim 10^{53}$ erg/s. This strong peak is illustrated as follows. As a supernova shock moves outward, it dissociates nuclei into free nucleons, which triggers deleptonization process $e^-p \rightarrow \nu_en$; these ν_e build up a sea because they are trapped and advected with matter. When the shock crosses the ν_e neutrinosphere, within which the created ν_e are trapped, they are abruptly emitted. For the other flavours $\bar{\nu}_e$ and ν_x , there is no such a sudden burst; both luminosities glow rather gradually and they are similar to each other. Usually, for both the pure MSW effect and the RSF effect with normal hierarchy, the most easily detected flavour $\bar{\nu}_e$ are transformed from original $\bar{\nu}_e$ and ν_x [14, 15]. Thus, luminosity curve does not provide any useful information on the flavour conversion mechanism. On the other hand, for the RSF effect with inverted mass hierarchy, the conversion $\nu_e \rightarrow \bar{\nu}'_\tau \rightarrow \bar{\nu}_e$ is considered to occur via RSF-H and MSW-H (see table 1); we expect that this case can be distinguished from the luminosity curve.

The other characteristic that provides information on flavour conversion mechanism is hierarchy of the average energy $\langle E_{\nu_e} \rangle < \langle E_{\bar{\nu}_e} \rangle < \langle E_{\nu_x} \rangle$ as clearly seen from figure 2; flavour conversions also cause the spectral exchange. This energy hierarchy is explained as follows. Since ν_x interact with matter only through the neutral-current interactions in supernovae, they are weakly coupled with matter compared to ν_e and $\bar{\nu}_e$. Thus the

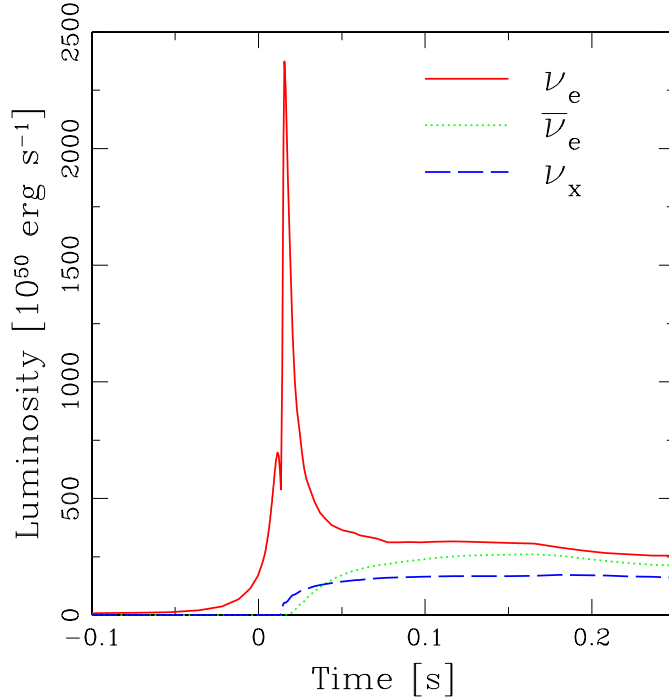


Figure 1. The original luminosity of the emitted neutrinos as a function of time, calculated by Thompson *et al* [19]. The progenitor mass is $15M_{\odot}$.

neutrinosphere of ν_x locates at deeper in the core than that of ν_e and $\bar{\nu}_e$, which leads to higher temperatures for ν_x . The difference between ν_e and $\bar{\nu}_e$ comes from the fact that the core is neutron-rich and ν_e couple with matter more strongly, through $\nu_e n \rightarrow e^- p$ reaction.

3.2. Presupernova profiles

We use the precollapse model of massive stars of Woosley and Weaver [16]. The model is $15M_{\odot}$ progenitor star with solar metallicity and it is labeled as W95S. The density and Y_e profiles are quite important for the flavour conversions because they determine the resonance regions as well as whether it is adiabatic or not. We show in figure 3 the $|\rho(1 - 2Y_e)|$ (responsible for RSF) and ρY_e profiles (responsible for MSW) of the W95S model. We also show $\Delta_{12} \equiv m_N \Delta m_{12}^2 \cos 2\theta_{12} / 2\sqrt{2}G_F E_{\nu}$ and $\Delta_{13} \equiv m_N |\Delta m_{13}^2| \cos 2\theta_{13} / 2\sqrt{2}G_F E_{\nu}$ as two horizontal bands (the bandwidth comes from the energy range 5–70 MeV). At intersections between Δ_{12}, Δ_{13} and $|\rho(1 - 2Y_e)|, \rho Y_e$, the RSF and MSW conversions take place.

In the previous publication, we have investigated the dependence on presupernova models [15]; in the paper, we have also used recent $15M_{\odot}$ presupernova models by Woosley *et al* [17] with both solar and zero metallicity (W02S and W02Z, where ‘S’ and ‘Z’ denotes solar and zero metallicity, respectively). This is because the RSF conversion

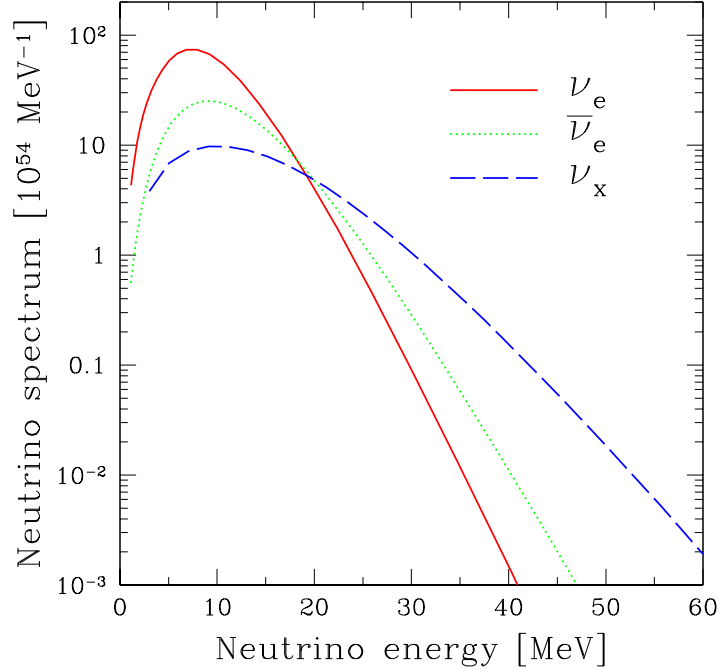


Figure 2. Original neutrino spectrum integrated to 0.25 s after core bounce, calculated by Thompson *et al* [19]. The progenitor mass is $15M_{\odot}$.

is very sensitive to the deviation of Y_e from 0.5 (see equation (4)), which strongly depends on the metallicities as well as on the weak interaction rates adopted in the simulation of stellar evolution. In fact, for the W02 models, in which the authors adopted more updated weak rates, the $|\rho(1-2Y_e)|$ profiles suddenly drop at RSF region, yielding rather nonadiabatic conversions; these properties are shown in figure 4. Nevertheless, we use the W95S model as our reference model because of the reasons listed below. First, since the conversion probabilities in RSF-H is highly adiabatic when the magnetic field is sufficiently strong (section 5), it is easier for us to investigate the dependence on mass hierarchy. Second, although the W02 models were calculated using a recent shell model and resulted in substantial revisions to the older data sets in the W95S model, there are still many uncertainties concerning nuclear physics; thus, these models cannot be considered to be decisive one. Finally, as discussed in the previous paper [15], because the lifetime of massive stars which end their life by gravitational collapse is much shorter than that of the Sun, the progenitors of the galactic supernovae are considered to be younger than the Sun, and therefore, more metal rich. Because the deviation of Y_e from 0.5 is determined by rarely existent nuclei, the suppression of $(1-2Y_e)$ will be weaker and the RSF conversion will incline to be more adiabatic, even if W02S model is the correct one of the progenitor with solar metallicity.

Although we use static progenitor models in calculating the flavour transition, in

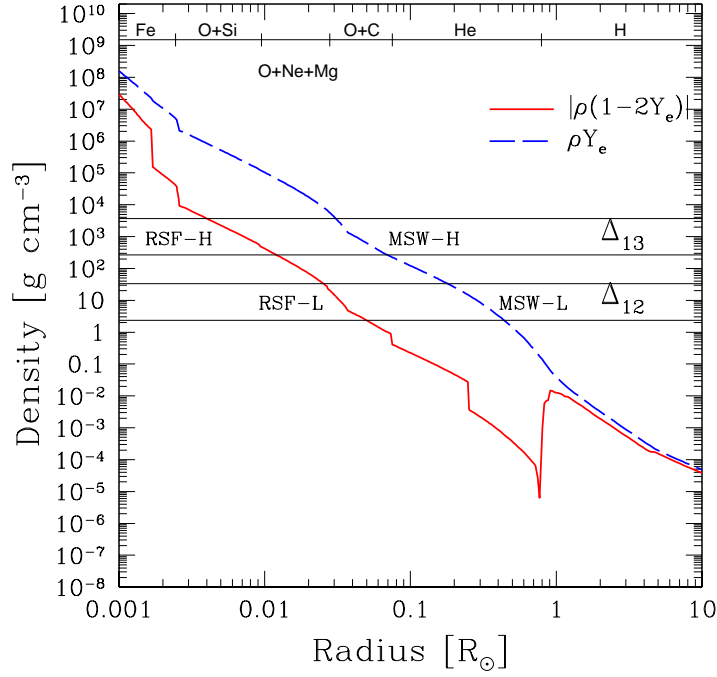


Figure 3. Presupernova profiles (W95S) used in our calculations, which is calculated by Woosley and Weaver [16]. The density and Y_e combination that is responsible for the RSF conversions $[\rho(1 - 2Y_e)]$, and that for the MSW conversions (ρY_e) . Two horizontal bands represent Δ_{12} and Δ_{13} (these definitions are given in the text); at the intersections between them and the profile curves, the RSF and MSW conversions occur.

fact the density profile changes drastically during a neutrino burst (~ 10 s) owing to shock wave propagation. However, our particular interest is within first 0.25 s after core bounce because the calculation of original neutrino emission [19] ends at that time (3.1). In the previous paper, we have already shown that until 0.25 s, using the static presupernova and magnetic field models is considered to be a good approximation [14]; this is based on the numerical calculation of the Lawrence Livermore group, which is the only group succeeding the shock propagation into the outer envelope.

3.3. Magnetic fields

We assume that the global structure of the magnetic field is a dipole moment and the field strength is normalized at the surface of the iron core with the values 10^{10} G (nearly complete RSF conversion) as well as 0 G (pure MSW conversion). The reason for this normalization is as follows. The magnetic fields should be normalized by fields that are static and exist before the core collapse, because those of a nascent neutron star can hardly affect the far outer region, where the RSF conversions take place, within the short time scale of a neutrino burst. As discussed in the previous subsection, since

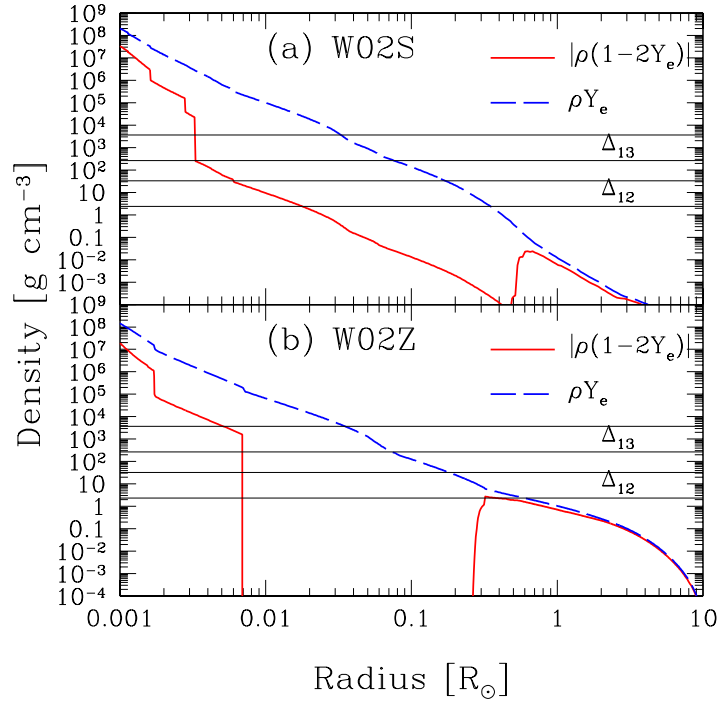


Figure 4. The same as figure 3 but for (a) W02S and (b) W02Z models.

the shock wave does not affect the resonance region at $\lesssim 0.25$ s after bounce, it is also expected that the magnetic field structure and strength at the resonance points are not seriously changed at that time. The strength of such magnetic fields above the surface of the iron core may be inferred from observations of the surface of white dwarfs, since both are sustained against gravitational collapse by the degenerate pressure of electrons. Observations of the magnetic fields in white dwarfs show that the strength spreads in a wide range of 10^7 – 10^9 G [20]. Considering the possibility of the decay of magnetic fields in white dwarfs, it is not unnatural to consider magnetic fields up to 10^{10} G at the surface of the iron core. Then, in equation (8), $B_{\perp} = B_0(r_0/r)^3 \sin \Theta$, where B_0 is the strength of the magnetic field at the equator on the iron core surface, r_0 the radius of the iron core, and Θ the angle between the pole of the magnetic dipole and the direction of neutrino propagation. Hereafter, we assume $\sin \Theta = 1$.

3.4. Neutrino parameters

We adopt the realistic neutrino mixing parameters inferred from the recent experimental results: for the atmospheric neutrino parameters, $|\Delta m_{13}^2| = 2.8 \times 10^{-3} \text{ eV}^2$, $\sin^2 2\theta_{23} = 1.0$, and for the solar neutrino parameters, $\Delta m_{12}^2 = 5.0 \times 10^{-5} \text{ eV}^2$, $\tan^2 \theta_{12} = 0.42$.

As for still uncertain neutrino properties, we must set some assumptions, e.g., whether the mass hierarchy is normal or inverted, as well as θ_{13} is large, enough for the MSW-H conversion to be adiabatic, or not. There is also uncertainty concerning the

Table 2. Models considered in this paper, concerning the neutrino properties.

Model	B_0 [G]	Mass hierarchy	$\sin^2 2\theta_{13}$
MSW-NOR-S	0	Normal	10^{-6}
MSW-NOR-L	0	Normal	0.04
MSW-INV-S	0	Inverted	10^{-6}
MSW-INV-L	0	Inverted	0.04
RSF-NOR-S	10^{10}	Normal	10^{-6}
RSF-NOR-L	10^{10}	Normal	0.04
RSF-INV-S	10^{10}	Inverted	10^{-6}
RSF-INV-L	10^{10}	Inverted	0.04

neutrino magnetic moment tensor μ_{ij} ; however, since the only relevant parameter is $\mu_{ij}B$, this uncertainty is already included in that of the magnetic field strength ($\mu_{ij} = 10^{-12}\mu_B$ is assumed). Thus, there are 8 parameter sets due to: whether the magnetic field is zero (label by ‘MSW’) or sufficiently strong $B_0 = 10^{10}$ G (‘RSF’); the mass hierarchy is normal (‘NOR’) or inverted (‘INV’); and $\sin^2 2\theta_{13} = 10^{-6}$ (‘S’) or $\sin^2 2\theta_{13} = 0.04$ (‘L’). We label one model by connecting these labels using hyphen, e.g., MSW-NOR-S. It should be particularly noticed that although we label the model with strong magnetic field simply by RSF-, it does not mean that the pure RSF effect occurs; every model labeled by RSF- is subject to both the MSW and RSF conversions. We summarize these models in table 2.

4. Qualitative conversion schemes

We qualitatively illustrate the conversion scheme for each model. Since $\bar{\nu}_e$ is the most easily detected flavour, we focus on the conversion channel that gives $\bar{\nu}_e$ appearance at the detector. Figure 5 schematically shows crossings among different mass eigenstates in matter, which is helpful for the reader to understand the qualitative discussions in this section.

4.1. Normal mass hierarchy

First, the case of the normal mass hierarchy is addressed (figure 5(a)); this case is minutely investigated in [14, 15], but we again repeat their discussion. When $B_0 = 0$, the produced $\bar{\nu}_e$ propagate the supernova envelope without experiencing the MSW resonance, and reach the stellar surface as the lightest mass eigenstate $\bar{\nu}_1$. The other mass eigenstates $\bar{\nu}_2, \bar{\nu}_3$ are originated from $\bar{\nu}_{\mu,\tau}$ whose flux is considered to be the same at the leading order. Thus, the $\bar{\nu}_e$ flux at the detector is described by

$$\begin{aligned}
 F_{\bar{\nu}_e} &= |U_{e1}|^2 F_{\bar{\nu}_1} + |U_{e2}|^2 F_{\bar{\nu}_2} + |U_{e3}|^2 F_{\bar{\nu}_3} \\
 &= |U_{e1}|^2 F_{\bar{\nu}_e}^0 + (1 - |U_{e1}|^2) F_{\nu_x}^0,
 \end{aligned}
 \tag{14}$$

where F^0 and F are the flux at production and detection, respectively. Since the parameter θ_{13} is essential for the MSW-H conversion, the results are not sensitive to the

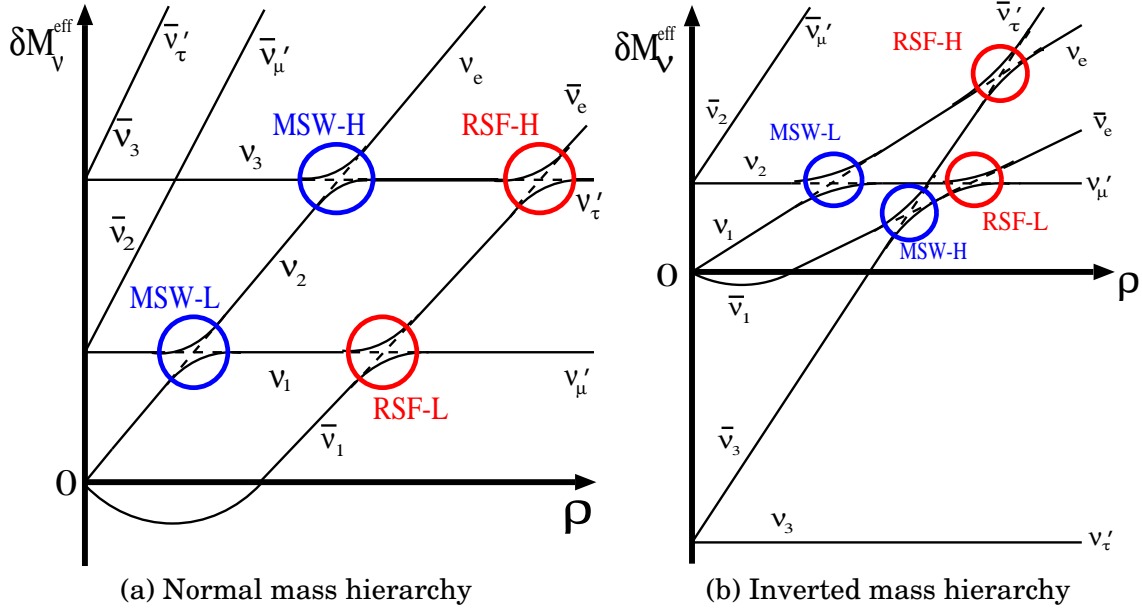


Figure 5. Schematic illustration of level crossings for (a) normal and (b) inverted mass hierarchy. In this figure, adiabatic conversion means that the neutrinos trace the solid curve at each resonance point, while nonadiabatic conversion is shown by the dashed line.

value of θ_{13} .

On the other hand, when $B_0 = 10^{10}$ G, RSF-H becomes almost completely adiabatic, whereas RSF-L is highly nonadiabatic. At the RSF-H point, the original ν'_τ are converted into $\bar{\nu}_e$, which propagate as the mass eigenstate owing to the large matter potential. These $\bar{\nu}_e$, then, cross the nonadiabatic RSF-L region (which gives no essential effects) and escape from the star as $\bar{\nu}_1$. The other mass eigenstates are also originated from ν_x , thus yielding

$$F_{\bar{\nu}_e} = F_{\nu_x}^0. \quad (15)$$

The value of θ_{13} does not matter also in this case. In consequence, the models MSW-NOR-S,L are characterized by equation (14), whereas, RSF-NOR-S,L are characterized by equation (15).

4.2. Inverted mass hierarchy

The situation changes dramatically in the case of the inverted mass hierarchy (figure 5(b)). The pure MSW effect in this case has been studied in detail in the literatures [2, 3]; the value of θ_{13} is critical for completeness of the conversions. The $\bar{\nu}_e$, which are produced as the lightest mass eigenstate in three antineutrino states, then cross the MSW-H resonance region. If this resonance is nonadiabatic (MSW-INV-S), the flavour conversion does not take place at the MSW-H point, i.e., $\bar{\nu}_e \rightarrow \bar{\nu}_1$. This case yields the $\bar{\nu}_e$ flux characterized by equation (14), which has already appeared. On the

Table 3. Conversion scheme for each model. In the second column, the most relevant conversion channel, which eventually results in $\bar{\nu}_1$, is given. The flux equation which is relevant for each model is summarized in the third column, and then the models are categorized into groups labeled by A, B, and C, as shown in the fourth column.

Model	Relevant conversion	Flux at the Earth	Group
MSW-NOR-S	$\bar{\nu}_e \rightarrow \bar{\nu}_1$	Equation (14)	A
MSW-NOR-L	$\bar{\nu}_e \rightarrow \bar{\nu}_1$	Equation (14)	A
MSW-INV-S	$\bar{\nu}_e \rightarrow \bar{\nu}_1$	Equation (14)	A
MSW-INV-L	$\bar{\nu}'_\tau \rightarrow \bar{\nu}_e \rightarrow \bar{\nu}_1$	Equation (15)	B
RSF-NOR-S	$\nu'_\tau \rightarrow \bar{\nu}_e \rightarrow \bar{\nu}_1$	Equation (15)	B
RSF-NOR-L	$\nu'_\tau \rightarrow \bar{\nu}_e \rightarrow \bar{\nu}_1$	Equation (15)	B
RSF-INV-S	$\bar{\nu}_e \rightarrow \bar{\nu}_1$	Equation (14)	A
RSF-INV-L	$\nu_e \rightarrow \bar{\nu}'_\tau \rightarrow \bar{\nu}_e \rightarrow \bar{\nu}_1$	Equation (18)	C

other hand for the MSW-INV-L model, MSW-H is completely adiabatic, and therefore the conversions $\bar{\nu}_e \rightarrow \bar{\nu}'_\tau \rightarrow \bar{\nu}_3$ as well as $\nu_x \rightarrow \bar{\nu}_{1,2}$ occur, which results in

$$F_{\bar{\nu}_e} = (1 - |U_{e3}|^2)F_{\nu_x}^0 + |U_{e3}|^2F_{\bar{\nu}_e}^0. \quad (16)$$

Since the value of θ_{13} (or $|U_{e3}|^2$) is strongly constrained to be very small by the reactor experiment [21], this expression essentially the same as the previous one (15).

When $B_0 = 10^{10}$ G (RSF-INV-S,L), the $\nu_e \leftrightarrow \bar{\nu}'_\tau$ conversion takes place at the RSF-H region. This $\bar{\nu}'_\tau$ further enter the MSW-H region. If this MSW resonance is nonadiabatic (-S model), these $\bar{\nu}'_\tau$ becomes $\bar{\nu}_3$ at the stellar surface. The other relevant conversions are the same as the pure MSW model $\bar{\nu}_e \rightarrow \bar{\nu}_1, \bar{\nu}'_\mu \rightarrow \bar{\nu}_2$. Thus, the $\bar{\nu}_e$ flux is given by

$$F_{\bar{\nu}_e} = |U_{e1}|^2F_{\bar{\nu}_e}^0 + |U_{e2}|^2F_{\nu_x}^0 + |U_{e3}|^2F_{\nu_e}^0, \quad (17)$$

which is almost the same as equation (14). On the other hand, for -L model, the mass eigenstates $\bar{\nu}'_\tau$ converted from ν_e reach the supernova surface as $\bar{\nu}_1$, because the adiabatic MSW-H conversion $\bar{\nu}'_\tau \leftrightarrow \bar{\nu}_e$ takes place. With the remaining channels $\bar{\nu}'_\mu \rightarrow \bar{\nu}_2, \bar{\nu}_e \rightarrow \bar{\nu}_3$, the observed flux is

$$F_{\bar{\nu}_e} = |U_{e1}|^2F_{\nu_e}^0 + |U_{e2}|^2F_{\nu_x}^0 + |U_{e3}|^2F_{\bar{\nu}_e}^0. \quad (18)$$

Consequently, the models MSW-INV-S and RSF-INV-S are characterized by equation (14), MSW-INV-L is by (15) and RSF-INV-L is by (18).

In table 3, we summarize the relevant conversions stated above for each model. Although there are eight models and this rather large number is expected to complicate the discussion, each model is consequently categorized into one of three groups A, B or C, as indicated in table 3. Fortunately, this greatly reduces the complexity, but within one group, we cannot specify each model by the SK observation.

5. Results of numerical calculations

5.1. Conversion probability

We calculated equation (8) numerically with the models given in section 3, and obtained the conversion probabilities for each flavour. Figure 6(a) shows the conversion probabilities of original ν_μ as a function of radius for the RSF-NOR-L model; the neutrino energy is 25 MeV. Because the ν_μ state is not mass eigenstate and maximally mixing with ν_τ , the probability $P(\nu_\mu \rightarrow \nu_\mu)$ should oscillate abruptly. In our calculation, however, we have averaged out this local behaviour, since we are only interested in the global change of the probabilities which is concerned with resonance. Therefore, the ν_μ survival probability starts from 0.5 rather than 1, because of the maximal mixing with ν_τ . A significant amount of ν_μ change into $\bar{\nu}_e$, owing mainly to the RSF-H conversion which occurs around $\sim 0.01R_\odot$, and the converted $\bar{\nu}_e$ propagates as the mass eigenstate due to matter effect, not being disturbed by further resonances, to $\sim 0.1R_\odot$. Around this radius, $\bar{\nu}_e$ start to mix with other flavour antineutrinos, reducing the probability $P(\nu_\mu \rightarrow \bar{\nu}_e)$. In figure 6(b), we show the conversion probabilities of original ν_e for the RSF-INV-L model. As already discussed in 4.2, the original ν_e are transformed into $\bar{\nu}_{\mu,\tau}$ at RSF-H, and they further change to the favoured flavour $\bar{\nu}_e$ in the MSW-H resonance point.

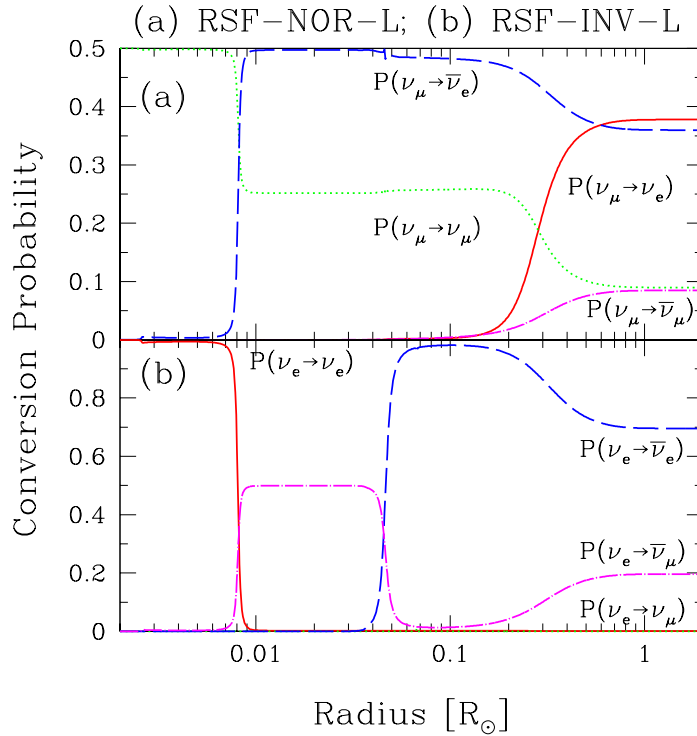


Figure 6. Conversion probabilities as a function of radius for (a) the RSF-NOR-L and (b) RSF-INV-L models. The injected neutrino energy is taken to be 25 MeV.

We show in figure 7 the same probabilities as those shown in figure 6, but the assumed value of θ_{13} is small ((a) RSF-NOR-S; (b) RSF-INV-S). Figure 7(a) indicates that the conversion probabilities from the original ν_μ are almost the same as those for RSF-NOR-L model; as we have already noted, the value of θ_{13} does not matter in the case of normal mass hierarchy. On the other hand, the behaviours in figure 7(b) is substantially different from those in figure 6(b). In particular, the most easily detected flavour $\bar{\nu}_e$ is not produced from the original ν_e . All these characteristics are consistent with the simple discussions given in section 4.

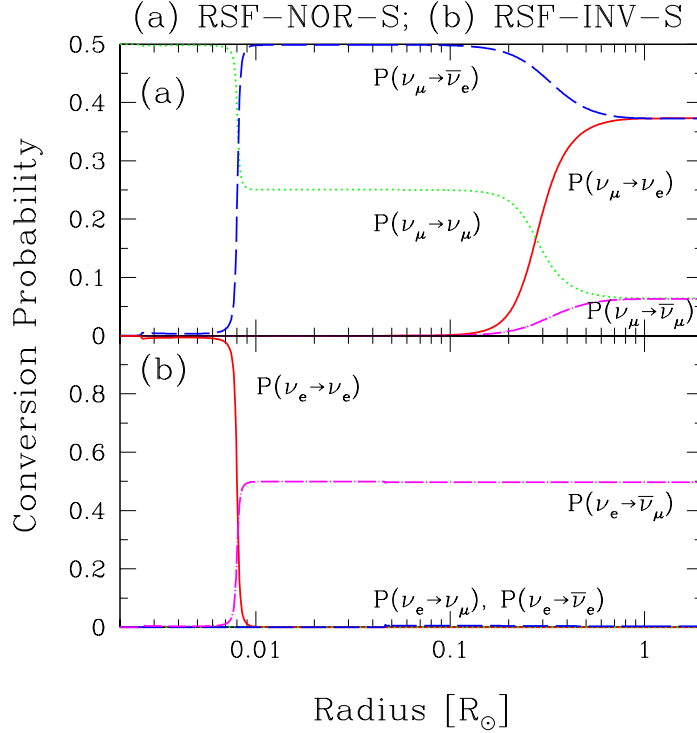


Figure 7. The same as figure 7, but for (a) the RSF-NOR-S and (b) RSF-INV-S models.

5.2. Neutrino signals at the Super-Kamiokande detector

With the conversion probabilities given in the previous subsection and the original neutrino spectrum by Thompson *et al* [19], we calculated the flux of each flavour neutrinos on the Earth. (From this point on, we assume the galactic supernova neutrino burst and take 10 kpc as a distance to the supernova.) Using this flux and the cross section of the relevant neutrino interaction at SK as well as the sensitivity of the detector, we can calculate the expected event numbers from a future galactic supernova neutrino burst. In this paper, we adopt the most dominant reaction $\bar{\nu}_e p \rightarrow e^+ n$ alone; a cross section of the reaction has been calculated in detail [22].

Figure 8(a) shows time evolution of the energy-integrated event as a function of

time for each group A, B and C, and we show the same in figure 8(b) but using equally spaced bins. From the time evolution of neutrino events, we cannot discern the groups A and B, because they show almost the same time profile. For group C, however, since the original ν_e are converted into $\bar{\nu}_e$, the time profile shows steep neutronization peak, and the event number contained in this peak is expected to be statistically significant as clearly seen in figure 8(b); the event number included in the most prominent three bins is ~ 180 . If the neutronization peak were actually obtained, it strongly indicates that the model group C would be favoured; since the group C contains only one model, RSF-INV-L, a great number of problems concerning the neutrino properties would be solved at the same time. In that case, the neutrino would have the nonzero magnetic moment, the mass hierarchy would be inverted, and the value of θ_{13} would be large enough for MSW-H to be adiabatic.

The expected event number per unit energy range, which is integrated during the first 0.25 s after core bounce, is shown in figures 8(c) and 8(d), in units of counts/MeV and counts/bin, respectively. From these figures, the model group C gives the softest spectrum, while B the hardest and A an intermediate one. In addition to the time evolution of the neutrino events, the number spectrum would provide useful information on the flavour conversion mechanism. Although the available data are restricted in order to avoid uncertainties concerning shock wave propagation, the obtained data would be statistically significant. Using the spectrum, degeneracy between the group A and B is expected to be broken.

6. Discussion

6.1. How far can we probe the neutrino properties from the supernova neutrino observation?

The expected neutrino signal at the SK detector has been investigated thus far. However, the mechanism of supernova explosions is quite unclear, since all the reliable numerical simulations have not succeeded in pushing the shock wave to penetrate the entire core. There may be several unknown processes which we have omitted so far, and the original neutrino spectrum as well as its luminosity curve are still controversial. Therefore, we cannot trust characteristics of the calculation by Thompson *et al* [19] in detail. Instead, we use rather simple quantities in order to discuss the conversion mechanisms from the neutrino signals; this approach is expected to considerably reduce the dependence on supernova models.

We adopt the following quantities:

$$R_{\text{SK}}^{\text{E}} = \frac{\text{Number of events for } E_e > 25 \text{ MeV}}{\text{Number of events for } E_e < 15 \text{ MeV}}, \quad (19)$$

$$R_{\text{SK}}^{\text{T}} = \frac{\text{Number of events for } 0 < t/\text{ms} < 75}{\text{Number of events for } 75 < t/\text{ms} < 150}, \quad (20)$$

in order to represent the spectral hardness and the peak sharpness of neutronization burst, respectively. Since the time of the core collapse would never known with the

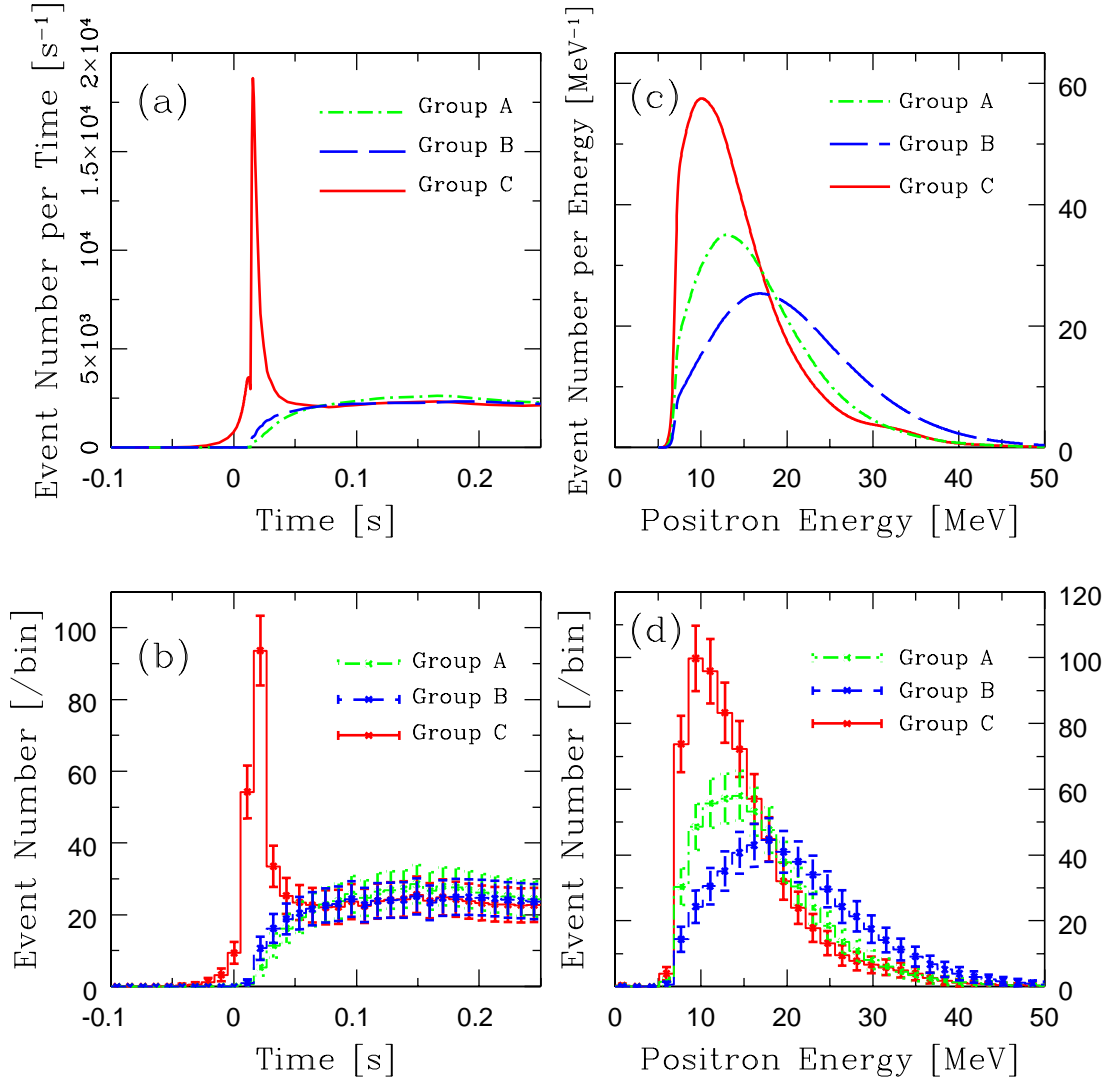


Figure 8. Neutrino signal at the SK detector, which is evaluated for model groups A, B and C: (a) Time evolution of the neutrino signal in unit of [counts/s]; (b) the same as (a), but in unit of [counts/bin] with 1σ statistical error bars; (c) number spectrum of positrons for first 0.25 s after core bounce in unit of [counts/MeV]; (d) the same as (c), but in unit of [counts/bin] with 1σ statistical error bars.

neutrino signal alone, we take time origin $t = 0$ when the first neutrino signal is detected. The place of the model groups A, B and C on the $(R_{\text{SK}}^E, R_{\text{SK}}^T)$ plane are shown in figure 9. These groups are well separated from each other, and we expect that this particular remains unchanged even if the adopted supernova model is different.

Although the degeneracy problem within each group cannot be solved by the SK observation, which mainly detect $\bar{\nu}_e$, it may be possible if ν_e could be detected efficiently. SNO is such a detector currently data taking with 1 000 tons of heavy water. The supernova ν_e can be detected via $\nu_e d \rightarrow e^- pp$ reaction. Although the $\bar{\nu}_e$ are also

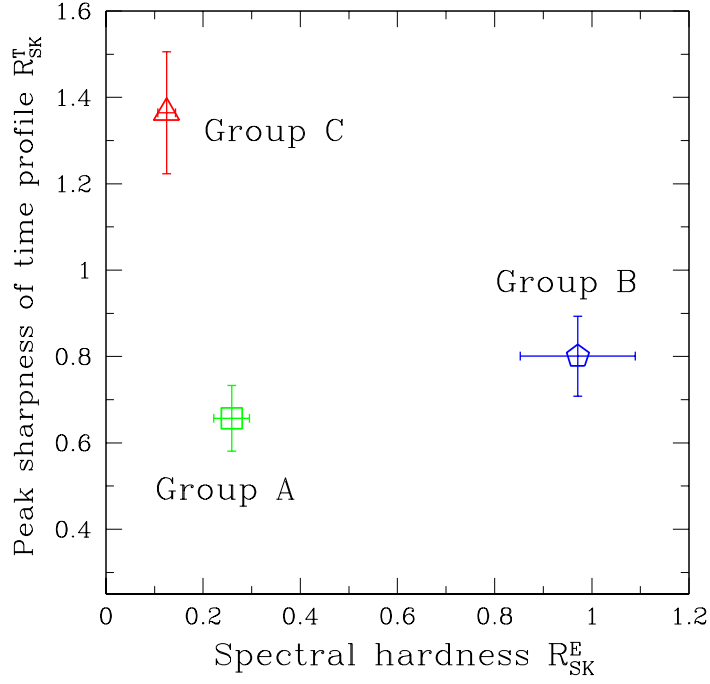


Figure 9. The model groups A, B and C, plotted on R_{SK}^E vs R_{SK}^T plane. The error bars include only statistical errors, and are at 1σ level.

detected through a similar reaction, $\bar{\nu}_e d \rightarrow e^+ nn$, these events could be discriminated using delayed coincidence technique. Thus at SNO, we expect that only ν_e signal can be extracted. Figure 10 is the same as figure 9 for the SNO detector, but is plotted for the models in (a) group A and (b) B. As shown in this figure, the degeneracy problem could be solved with the ν_e data in principle, but the current smallness of the SNO detector prevents a statistically significant discussion.

6.2. Dependence on presupernova models

Until this point, we have adopted the presupernova model W95S as our reference model. However, as already stated in 3.2 or investigated in [15], the RSF conversions are highly dependent on the presupernova profiles. In fact, figures 3 and 4 show that the relevant profile for the RSF effect, $\rho(1 - 2Y_e)$, is quite different among these models as well as their metallicities. On the other hand, the MSW conversions are insensitive to the presupernova models because their relevant profile is ρY_e that is not subject to the deviation of Y_e from 0.5. In particular for the W02 models, the value of $\rho(1 - Y_e)$ suddenly drops at the RSF-H region, yielding rather nonadiabatic conversions. Since RSF becomes incomplete but MSW does not change for these models, the model group B, which contains RSF-NOR-S, RSF-NOR-L and MSW-INV-L models, should be further divided into two subgroups; we define group B I containing two RSF models,

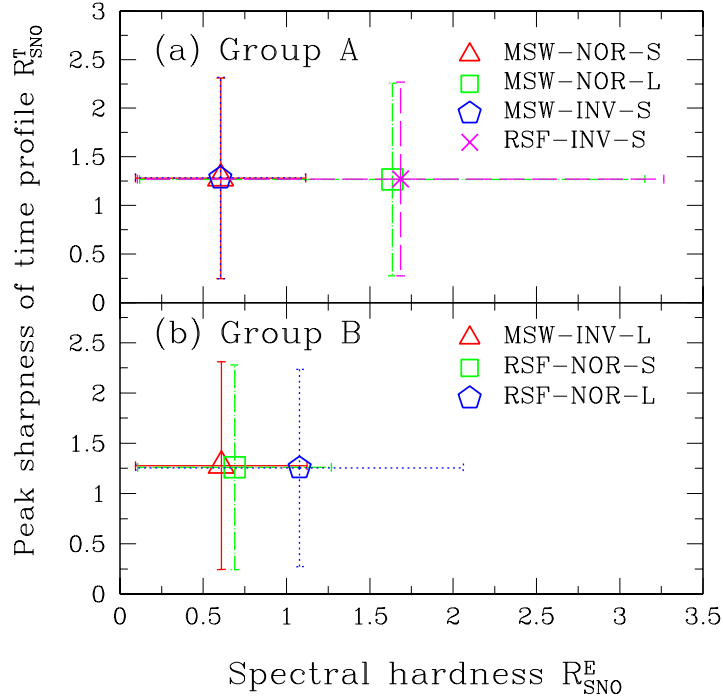


Figure 10. The same as figure 9, but for the SNO detector. The models are plotted within (a) groups A and (b) B.

while MSW-INV-L is named group B II. Consequently, we have four characteristic model groups A, B I, B II and C; in particular, the groups B II and C contain only one specific model each. Within each group, we cannot identify each model from the SK observation.

Figures 11(a) and (b) show time evolution of neutrino events at SK, calculated with the W02S and W02Z models. Comparing these figures with figure 8(a), the neutronization peak is not as sharp as that for the W95S model. This is because the RSF-H conversion is not efficient owing to sudden drop of the $\rho(1 - 2Y_e)$ profiles. However, since that peak is still prominent and statistically significant, the model group C would be discriminated from the other groups using the time profile detected at SK.

Figures 11(c) and (d) show the number spectrum of the neutrino signal, which is evaluated for the W02S and W02Z models, respectively. The spectra for groups A and B II are unchanged from the previous calculation with the W95S model (figure 8(c)), because they are essentially described by the pure MSW effect, which is insensitive to presupernova models. Therefore, we focus on the other two groups B I and C. For the group B I, the hardness of spectra locates between that of group A and B II, and it strongly depends on the adopted metallicities. More detailed discussions concerning this group have been already given in our previous paper [15], and we refer the reader to the literature. For the group C, the low energy peak disappears from the spectrum calculated with the W02S model, reflecting the $\rho(1 - 2Y_e)$ profile of the W02S model

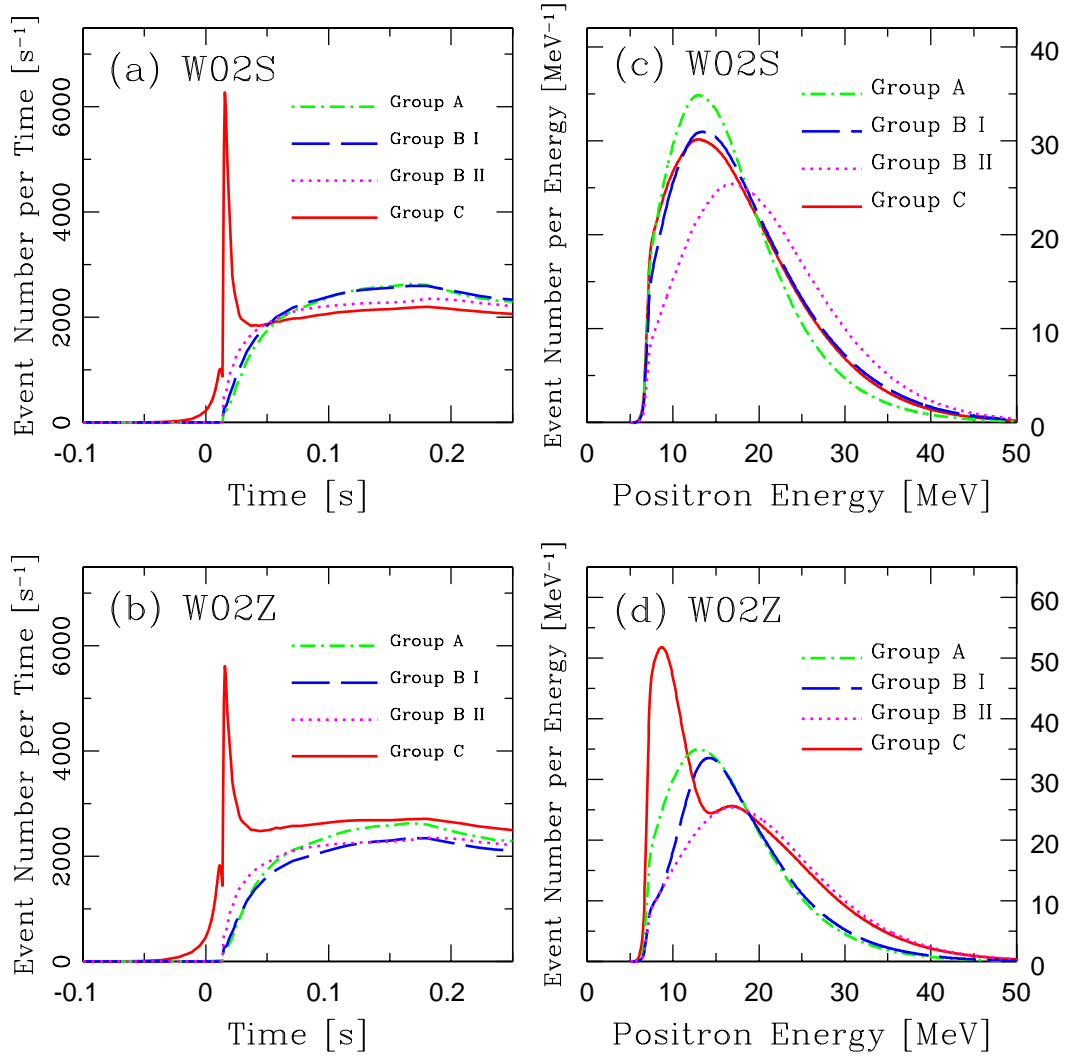


Figure 11. Time evolution and number spectrum of neutrino events calculated with W02S and W02Z models.

(figure 4(a)), which significantly reduces the efficiency of the RSF-H conversions. On the other hand, this low energy peak remains for the W02Z model, also reflecting the $\rho(1 - Y_e)$ profile. As clearly shown in figure 4(b), it mildly changes in the RSF-H region for low energy neutrinos. However, if the energy is beyond some critical value, RSF-H becomes completely nonadiabatic, because the $\rho(1 - 2Y_e)$ profile abruptly drops to zero. Thus, the $\nu_e \rightarrow \bar{\nu}_e$ conversion is highly efficient for low energy neutrinos but is highly inefficient for high energy ones; for the high energy region the $\nu_x \rightarrow \bar{\nu}_e$ conversion is relevant, which leads to double peak profile of the spectrum.

7. Conclusion

In this paper, we investigated the RSF conversions in supernovae for both the normal and inverted mass hierarchy. As the case for the pure MSW effect, we found that the RSF transitions are strongly dependent on the neutrino mass hierarchy, and also on the value of θ_{13} . We first gave qualitative discussion on the neutrino conversions including both the RSF and MSW effect, for eight parameter sets summarized in table 2. From that consideration, it was found that these models are categorized into only three groups, each of which is expected to show characteristic neutrino signal at the SK detector; we named these groups A, B and C, and which parameter set is included in each group is summarized in table 3.

We, then, presented results of numerical calculations of flavour conversions in supernova envelope. The density and Y_e profiles of the presupernova star calculated by Woosley and Weaver [16] (W95S) was adopted for the calculations. As the magnetic field structure, we assumed dipole-type and normalized its strength at the surface of the iron core. Using the conversion probabilities calculated by such a procedure and the original supernova neutrino spectrum as well as luminosity curve given by Thompson *et al* [19], the expected neutrino signal at the SK detector was estimated. As the result, it was found that there are clear difference between the model groups both for the spectral shape and the time evolution of the neutrino events. In particular, the model group C, which include the RSF-INV-L model alone, shows a sharp neutronization peak. Therefore, if this peak were detected in reality from the future galactic supernova neutrino burst, it would strongly support the RSF-INV-L model. It would indicate that many problems concerning the neutrino property should be solved at the same time, i.e., the neutrino have the nonzero magnetic moment, the mass hierarchy is inverted, and the value of θ_{13} is large enough to induce the adiabatic MSW-H resonance. From the spectral shape, it would be possible to discern the groups A and B, however, within each model group we need other information such as the signal of ν_e , to discriminate one model from the others. Although the SNO detector could detect ν_e efficiently, current smallness of the detector would prevent the statistically significant discussions.

We also studied the dependence on presupernova models. As already investigated in our previous paper [15], the RSF conversion is strongly dependent on the deviation of Y_e from 0.5, which is quite sensitive to the metallicities as well as the weak interaction rates adopted in the simulation of stellar evolution. The presupernova models by Woosley *et al* [17] (W02S and W02Z) shows the considerably different $\rho(1 - 2Y_e)$ profile from that of the W95S model. For both models, there exists sudden drop of the $\rho(1 - 2Y_e)$ profile at the RSF-H region, which pushes the RSF conversion rather nonadiabatic, and the expected neutrino signal was found to be different from that estimated with the W95S model. Still, since the neutronization peak for the RSF-INV-L model exists at the statistically significant level, it would keep to be useful method also in these cases.

Acknowledgments

SA's work is supported by Grant-in-Aid for JSPS Fellows. KS's work is supported in part by Grant-in-Aid for Scientific Research provided by the Ministry of Education, Culture, Sports, Science and Technology of Japan through Research Grant No S14102004, Grant-in-Aid for Scientific Research on priority Areas No 14079202.

References

- [1] Raffelt G G, 2002 *Nucl. Phys. B (Proc. Suppl.)* **110** 254
- [2] Dighe A S and Smirnov A Y, 2000 *Phys. Rev. D* **62** 033007
- [3] Takahashi K and Sato K, 2003 *Prog. Theor. Phys.* **109** 919
- [4] Cisneros A, 1970 *Astrophys. Sp. Sci.* **10** 87
- [5] Fujikawa K and Shrock R E, 1980 *Phys. Rev. Lett.* **45** 963
- [6] Schechter J and Valle J W F, 1981 *Phys. Rev. D* **24** 1883
Schechter J and Valle J W F, 1982 *Phys. Rev. D* **25** 283(E)
- [7] Lim C S and Marciano W J, 1988 *Phys. Rev. D* **37** 1368
Akhmedov E K, 1988 *Sov. J. Nucl. Phys.* **48** 382
Akhmedov E K, 1988 *Phys. Lett. B* **213** 64
- [8] Wolfenstein L, 1978 *Phys. Rev. D* **17** 2369
Mikheyev S P and Smirnov A Y, 1985 *Sov. J. Nucl. Phys.* **42** 913
Mikheyev S P and Smirnov A Y, 1986 *Nuovo Climento C* **9** 17
- [9] Barranco J, Miranda O G, Rashba T I, Semikoz V B and Valle J W F, 2002 *Phys. Rev. D* **66** 093009
Chauhan B C and Pulido J, 2002 *Phys. Rev. D* **66** 053006
- [10] Eguchi K *et al* , 2003 *Phys. Rev. Lett.* **90** 021802
- [11] Torrente-Lujan E, 2003 *J. High Energy Phys.* JHEP04(2003)054
Chauhan B C, Pulido J and Torrente-Lujan E, 2003 *Phys. Rev. D* **68** 033015
- [12] Ayala A, D'Olive J C and Torres M, 1999 *Phys. Rev. D* **59** 111901
- [13] Voloshin M B, 1988 *Phys. Lett. B* **209** 360
Akhmedov E K and Berezhiani Z G, 1992 *Nucl. Phys. B* **373** 479
Akhmedov E K, Petcov S T and Smirnov A Y, 1993 *Phys. Rev. D* **48** 2167
Peltoniemi J T, 1992 *Astron. Astrophys.* **254** 121
Athar H, Peltoniemi J T and Smirnov A Y, 1995 *Phys. Rev. D* **51** 6647
Totani T and Sato K, 1996 *Phys. Rev. D* **54** 5975
Nunokawa H, Qian Y Z and Fuller G M, 1997 *Phys. Rev. D* **55** 3265
Nunokawa H, Tomàs R and Valle J W F, 1999 *Astropart. Phys.* **11** 317
- [14] Ando S and Sato K, 2003 *Phys. Rev. D* **67** 023004
- [15] Ando S and Sato K, 2003 *Phys. Rev. D* **68** 023003
- [16] Woosley S E and Weaver T A, 1995 *Astrophys. J. Suppl. Ser.* **101** 181
- [17] Woosley S E, Heger A and Weaver T A, 2002 *Rev. Mod. Phys.* **74** 1015
- [18] Ahriche A and Mimouni J, 2003 *Preprint astro-ph/0306433 v1*
- [19] Thompson T A, Burrows A and Pinto P, 2003 *Astrophys. J.* **592** 434
- [20] Ghanmugam G, 1992 *Ann. Rev. Astron. Astrophys.* **411** 823
- [21] Apollonio M *et al* , 1999 *Phys. Lett. B* **466** 415
- [22] Vogel P and Beacom J F, 1999 *Phys. Rev. D* **60** 053003
Strumia A and Vissani F, 2003 *Phys. Lett. B* **564** 42